JURNAL OF BALKANI GEOPHYSICAL SOCIETY, Vol. 7, No.3, August, 2004, p. 23 – 29

Attenuation in the uppermost inner core from PKP data observed at Romanian stations

Marian Ivan* and Mihaela Popa **

* Dept.of Geophysics, University of Bucharest, 6 Traian Vuia str., 70138 Bucharest o.p.37, Romania.
e-mail: ivam@gg.unibuc.ro
** National Institute for Earth Physics, P.O.Box MG-2, 76900 Bucharest, Romania.

Abstract: *The Q_P factor at the top of the inner core is using PKPdf and PKPbc phases recorded at Romanian stations from some strong deep Fiji earthquakes. The amplitude spectral ratio method is used. The derived mean value of Q_P is 295 ± 20 (95% confidence level). The sampled region of the inner core is centered beneath the Japan Sea and the maximum depth of penetration of the PKPdf phase into the inner core is roughly 254 km. A slight increase of Q_P with depth is observed, although not resolvable, given the data scattering.*

Key words*: PKP-phases attenuation, amplitude spectral ratio, Q_P factor, inner core*

INTRODUCTION

Over the last three decades, the attenuation of high frequency P-waves in the inner core (IC) has been extensively studied, providing constraints on the core structure and nature (e.g. Souriau et al., 2003). While heterogeneity and anisotropy of the IC are well-documented by various studies on travel times, the radial and lateral variation of the IC quality factor Q_P, or its frequency dependency, are still elusive (e.g. Helffrich and Kaneshima, 2002). Most results to date have been restricted to a small number of processed events, or to an uneven distribution of earthquakes and recorders (e.g. Tseng et al., 2001). A summary of some previous inferences on Q_P is presented in Table 1.

Table 1. Synopsis of some previous inferences on Q_P.

Source	Depth behaviour of Q_P	Q_P range/value	Q_P behaviour in Frequency Band (0.2 - 2 Hz)
Doornbos (1974)	Variable (increasing with depth bellow Inner Core Boundary)	200 ÷ 600	Independent
Cormier (1981)	Constant	≈ 280	—
Niazi & Johnson (1992)	Compatible with a depth variation but not resolvable	176 (±10)	—
Tseng et al. (2001)	Variable	241 (±22) for depths < 210 km to 337 (±47) for depths > 270 km	Independent
	Geographical variation	Western Pacific 305 (±25) Eastern Pacific 160 (±34)	
Helffrich et al. (2002)	No trend with depth	130^{+225}_{-52} (between 140 - 340 km)	—
Present Paper	Compatible with a depth variation but not resolvable	295 (±20)	Independent

The seismological stations in the Balkans and surrounding areas are approximately 150° away from the majority of Fiji earthquakes. Consequently, core phases like PKPdf, PKPbc and PKPab (less frequently) are accurately observed, especially for strong, deep events (Fig. 1).

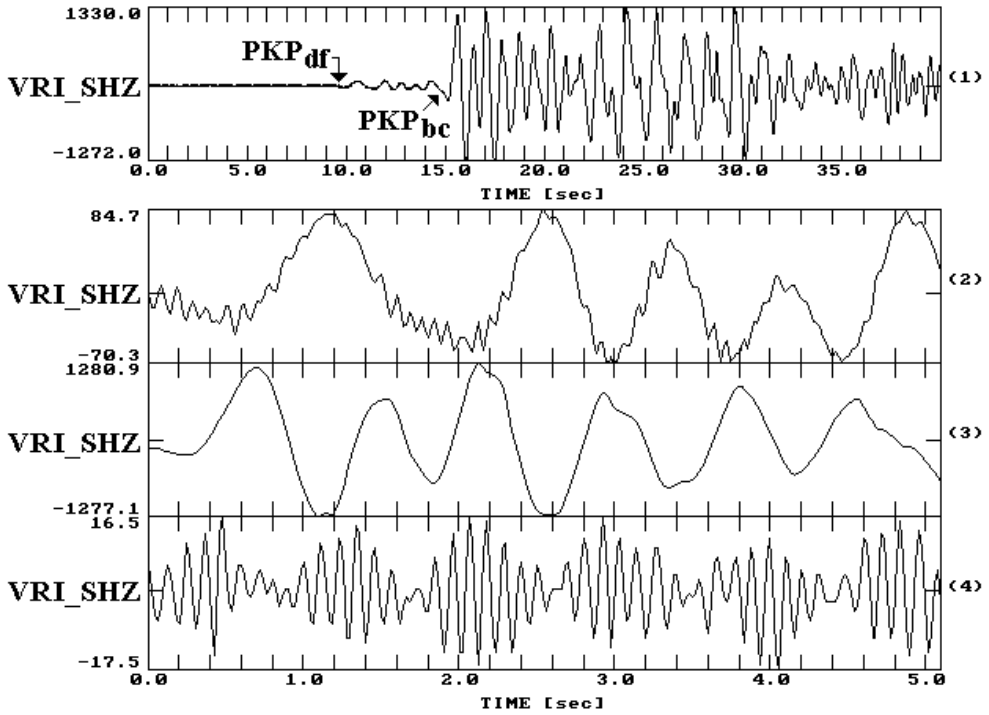

FIG. 1. Recording at Vrincioaia (VRI) station (Δ=148.2°) of 1998-05-16 earthquake (S13 vertical instrument at ~ 50 Hz sampling) (trace 1). Traces (2) and (3) are the time windows of 256 points immediately following the arrivals of PKPdf and PKPbc, respectively. Note the depletion in high frequencies of PKPdf phase relative to PKPbc, assumed to be a result of the attenuation in the inner core. The bottom trace is a noise window considered for reference.

The ray paths of the first two phases above are quite similar in the mantle, but differ in the core (Fig.2). While PKPdf penetrates ~300 km deep into the IC, PKPbc wave has the bouncing point just grazing the base of the outer core (e.g. Souriau et al., 2003).

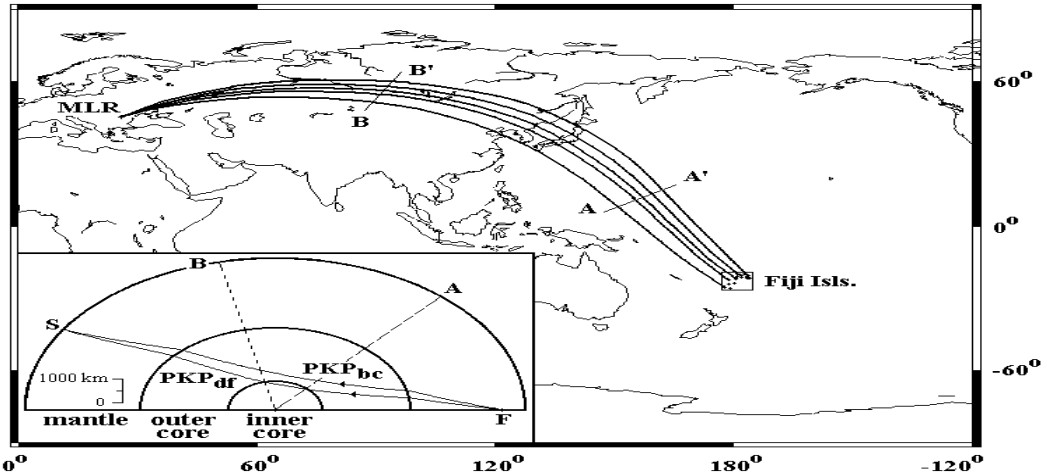

FIG. 2. Locations of the processed Fiji earthquakes. Solid lines show some representative surface projections of the ray paths to Muntele Rosu (MLR) station. The panel in the lower left corner shows the PKPdf and PKPbc paths for a deep event. Piercing points of the inner core boundary are indicated.

Because of the high attenuation (very low Q_P values) of seismic waves in the IC, PKPdf is routinely depleted of high frequencies compared to PKPbc. By using the standard spectral ratio method (e.g. Souriau and Roudil, 1995; Helffrich and Kaneshima, 2002), these phases make it possible to investigate attenuation properties at the top of the IC. In this paper, Q_P values are obtained from 23 major earthquakes ($M_w \geq 6$) in the Fiji area. These events were recorded at Muntele Rosu (MLR), a GEOFON station, from 1994 October 9th to 2003 October 7th. The station is equipped with an STS2 broad-band instrument. Where available, data from the K2 German-Romanian network (including a variety of sensors) (Bonjer et al., 2000), and from the short period Romanian telemetered stations (Teledyne Geotech S-13 instruments) have been also used. The hypocentral data of the processed events are summarized in Table 2, and the above stations are shown in Fig.3.

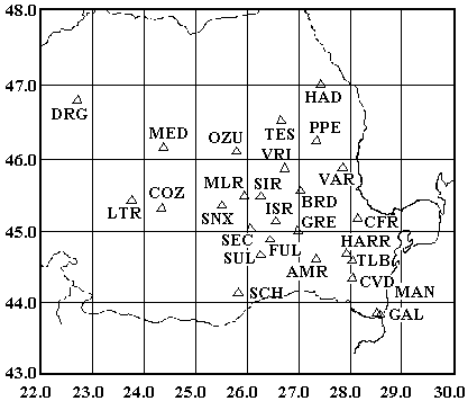

FIG. 3. Romanian stations used in this study.

Table 2. The hypocentral parameters of the processed events (source: NEIC or ISC).

No	Event	Time	Latitude (°)	Longitude (°)	Depth (km)	Mag.
1	94-10-27	22:20:28.54	-25.78	179.34	518	6.7
2	95-10-29	19:40:57.92	-21.79	-179.39	618	6.1
3	95-12-10	23:46:59.69	-21.51	-178.08	412	6.2
4	96-10-19	14:53:48.78	-20.41	-178.51	590	6.9
5	96-11-14	13:47:38.11	-21.24	-176.62	191	6.2
6	98-01-27	21:05:44.36	-22.41	179.04	610	6.5
7	98-04-14	03:41:22.33	-23.82	-179.87	498	6.1
8	98-05-16	02:22:02.64	-22.2067	-179.5049	571	6.9
9	98-07-19	15:58:38.86	-21.84	-175.79	72	6.1
10	98-11-15	02:44:12.38	-21.59	-176.5	149	6.3
11	98-12-27	00:38:26.51	-21.808	-176.3338	149	6.8
12	00-01-15	12:49:45.07	-21.22	-179.26	632	6.0
13	00-04-18	17:28:12.39	-20.66	-176.47	220	6.0
14	00-06-14	02:15:28.01	-25.626	178.058	631	6.4
15	00-09-02	17;02:19.55	-20.07	-179.13	687	6.0
16	00-12-18	01:19:21.31	-21.154	-179.115	618	6.6
17	01-05-19	17:36:25.59	-19.9	-177.51	368	6.0
18	01-07-04	07:06:30.93	-21.735	-176.727	179	6.5
19	01-09-12	08:48:37.91	-21.015	-179.06	611	6.4
20	02-10-04	19:05:48.77	-20.99	-179.02	621	6.3
21	02-12-10	04:27:54.60	-24.14	179.24	530	6.1
22	03-01-04	05:15:03.84	-20.57	-177.66	378	6.5
23	03-07-27	02:04:11.53	-21.08	-176.59	212	6.6

THEORETICAL BACKGROUND

It is generally assumed that amplitude spectra of recorded waves decrease exponentially with the frequency f, according to

$$A(f) = A_0 \exp(-\pi . t^* f) \quad , \qquad (1)$$

where A_0 is a constant and

$$t^* = \int_{\text{ray path}} \frac{dt}{Q} \quad , \qquad (2)$$

Considering the PKPdf and PKPbc phases, the logarithm of the amplitude spectra ratio will be linearly dependent on

frequency (Niazi and Johnson, 1992; Bhatttacharyya et al., 1993)

$$\ln\left[A_{DF}(f)/A_{BC}(f)\right] = C - \pi\left(t^*_{DF} - t^*_{BC}\right)f \quad , \qquad (3)$$

where C is a certain constant. Taking into account the very high values of Q in the outer core, the Q_P values in the inner core can been evaluated by

$$Q_P = \pi \frac{t_{PKPdf}}{S} \qquad (4)$$

where ***S*** is the absolute value of the slope of the regression line described by (3) and t_{PKPdf} is the propagation time of the PKPdf wave in the IC.

DATA AND METHODOLOGY

For each processed event, digital data retrieved by using **PITSA** software (Scherbaum and Johnson, 1992) have been carefully examined, and the observed arrival times of the PKP phases have been compared to the values derived using the IASP91 model (Buland and Chapman, 1983; Kennett and Engdahl, 1991). Generally, the (O-C) time residuals do not exceed 3 seconds. Phase polarity with respect to the fault plane solutions reported at **ISC** has been also considered. The investigated earthquakes show a variety of focal mechanisms and focal depths. In order to minimize scattering of the short-period amplitudes of the PKP phases, most of the processed events are deep. Also, only earthquakes with the projections of the PKP rays on the focal hemisphere sufficiently distant from nodal planes have been used (Cormier, 1981). The quality factor Q_P has been evaluated by using the routine methodology (e.g Roth et al., 1999). A constant-length window has been used to evaluate the natural logarithm of the amplitude spectra for each PKPdf and PKPbc phase. The window length is 128 points for the broad band instrument with sampling rate of 20 Hz, 256 points for telemetered stations at ~50 Hz sampling and 1024 points for K2 instruments at 200 Hz. In a few cases, the PKPdf window has been padded with a small number of zeroes. Usually, the above window length avoids the contamination of PKPbc by PKPab, but the latter has been clearly identified in a limited number of cases. A noise window of the same length, preceding the arrival of the PKPdf wave has been selected as reference. Spectral computations for PKPdf, PKPbc and noise windows have been performed by using the (input bit reversal) FFT subroutine described by Stearn (1975). In almost all cases, a clear change of the spectral slope around 2 Hz is observed (Fig. 4).

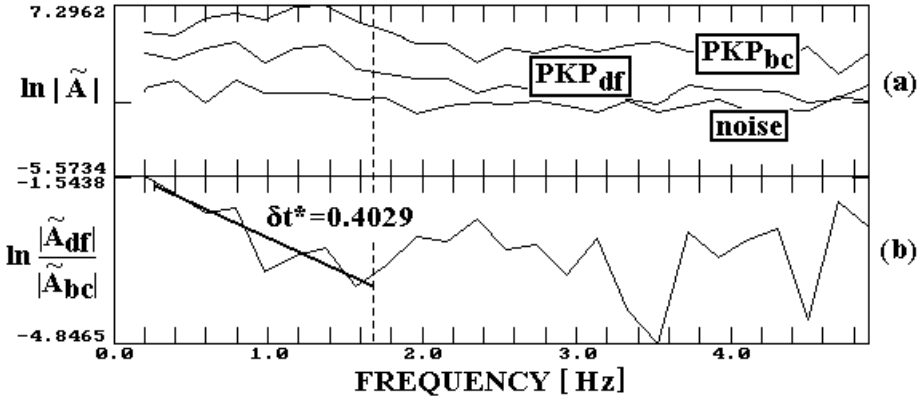

FIG. 4. Logarithm of the amplitude spectra for the time windows from Fig. 1 (below 5Hz). (a) spectra of PKP phases and of the noise; (b) difference df-bc. Note the linear decreasing below approximately 2 Hz, followed by a horizontal or upward trend.

Consequently, the computations have been performed in two or three frequency windows close to 0.2÷2 Hz, where the amplitude spectra of both PKP waves are clearly above noise spectrum and display a decreasing linear trend. The logarithm of the ratio of the spectral amplitudes of PKPdf to PKPbc has been computed and a linear regression has been estimated for each frequency window.

Finally, the Q_P value has been obtained from eq. (4). The propagation time of PKPdf in the inner core was evaluated using the **ak135** velocity model (Kennett et al., 1995). A statistical analysis has been subsequently performed in order to assess the confidence of the results.

No	Station	Instrument	Δ(°)	rBP (km)	Frequency band (Hz) / δt* (s)			Q
1	*MLR*	STS-2	151	963	A / 0.4525	B / 0.4955	-	256
	MLR	S-13			C / 0.4448	D / 0.5830	E / 0.6127	
	VRI	S-13	150.3	980	C / 0.4391	D / 0.4603	E / 0.4590	284
2	**MLR**	STS-2	148.5	1020	A / 0.3530	B / -	-	384
	MLR	S-13			C / -	D / 0.2185	E / 0.3539	
	SNX	S-13	148.9	1013	C / 0.4549	D / 0.3446	E / 0.4329	293
	TLB	S-13	147.9	1032	C / 0.6310	D / 0.5901	E / 0.5043	200
3	**MLR**	STS-2	149	1018	A / 0.2376	B / -	-	502
	CFR	S-13	148.0	1037	C / 0.2038	D / 0.2817	E / 0.2922	440
	COZ	S-13	149.9	993	C / 0.9286	D / 1.0051	E / 0.6743	144
	ISR	S-13	148.9	1019	C / 0.4259	D / 0.4010	E / 0.2702	325
	SNX	S-13	149.3	1009	C / 0.4330	D / 0.3876	H / 0.8807	214
4	**MLR**	STS-2	147.9	1035	A / 0.6302	B / 0.4955	-	265
	MLR	S-13			C / 0.4063	D / 0.3657	E / 0.2649	
	BRD	S-13	147.3	1046	H / 0.6309	-	-	176
	ISR	S-13	147.8	1036	C / 0.5457	D / 0.5715	E / 0.3712	230
	TLB	S-13	147.3	1045	C / 0.3597	D / 0.4283	E / 0.4110	279
	VRI	S-13	147.2	1047	C / 0.6813	D / 0.6296	E / 0.4932	184
5	**MLR**	STS-2	149.5	1011	A / 0.6194	B / 0.3265	-	256
	TLB	S-13	149.0	1022	C / 0.3924	D / 0.3250	-	329
6	**MLR**	STS-2	148.2	1028	A / 0.3622	B / 0.2866	-	359
	CFR	S-13	147.1	1048	C / 0.4423	D / 0.3595	E / 0.4414	267
	VRI	S-13	147.5	1041	C / 0.5022	D / 0.5232	E / 0.4887	224
7	**MLR**	STS-2	149.9	991	A / 0.5350	B / 0.2207	-	369
	MLR	S-13			C / 0.2822	D / 0.3385	E / 0.3320	
	CFR	S-13	148.8	1018	C / 0.3761	D / 0.3679	E / 0.3587	324
8	**MLR**	STS-2	148.8	1016	A / 0.3122	B / 0.2328	-	439
	BRD	S-13	148.2	1029	C / 0.2226 D / 0.2649	F / 0.2499 G / 0.3104	-	444
	CFR	S-13	147.8	1037	C / 0.3193 D / 0.4452	F / 0.3266 G / 0.4906	-	288
	ISR	S-13	148.7	1018	C / 0.6544 D / 0.6814	F / 0.4626 G / 0.4425	-	213
	PPE	S-13	147.3	1046	C / 0.2781 D / 0.2569	F / 0.3313 G / 0.3193	-	375
	VRI	S-13	148.2	1030	C / 0.2957 D / 0.2484	F / 0.4029 G / 0.3726	-	340
	FUL	S-13	148.9	1013	C / 0.5136	D / 0.4954	-	239
	HAD	S-13	147.1	1050	C / 0.6726	D / 0.7285	-	157
	MAN	S-13	148.3	1026	C / 0.5523	D / 0.5425	F / 0.6953	196
	SEC	S-13	149	1010	-	-	F / 0.6081	199
	TES	CMG3T	147.8	1037	-	D / 0.3511	F / 0.3303	334
	VAR	S-13	147.5	1042	-	D / 0.4564	F / 0.4952	236
	VRI	S-13	148.2		-	D / 0.2723	F / 0.4532	
9	**MLR**	STS-2	150.4	991	A / 0.4381	B / 0.3501	-	258
	MLR	S-13			C / 0.5451	D / 0.5562	E / 0.5518	
10	**MLR**	STS-2	149.9	1003	A / 0.31394	-	-	425

	MLR	S-13			C / 0.3069	D / 0.2476	-	
	COZ	S-13	150.8	980	C / 0.6639	D / 0.6059	E / 0.4716	221
	ISR	S-13	149.8	1004	C / 0.4322	D / 0.3521	-	313
11	**ISR**	S-13	150.1	997	C / 0.5748	D / 0.4645	-	239
	MLR	S-13	150.1	996	D / 0.4431	F / 0.4854		269
	SNX	S-13	150.4	989	C / 0.5938	D / 0.4169	-	250
	HAD	S-13	148.3	1037	D / 0.2525	F / 0.4648	-	317
	MAN	S-13	149.9	1003	D / 0.4282	F / 0.5271	-	258
	SUL	S-13	150.5	986	D / 0.3563	F / 0.5535		280
12	*MLR*	STS-2	148.1	1028	A / 0.4751	B / 0.4210	-	260
	TLB	S-13	147.6	1039	C / 0.4157	D / 0.4883	-	250
13	**MLR**	STS-2	149.1	1021	A / 0.3690	B / 0.3535	-	328
14	**MLR**	STS-2	150.1	981	A / 0.5327	B / 0.2471	-	296
	MLR	S-13			C / 0.5794	D / 0.3734	-	
	ISR	S-13	150.0	985	C / 0.2900	D / 0.1738	-	549
	SNX	S-13	150.4	973	C / 0.3355	D / 0.6038	-	278
	VRI	S-13	149.5	997	C / 0.6611	D / 0.5878	-	199
	HAD	S-13	148.4	1022	C / 0.4281	D / 0.4428	-	271
	VAR	S-13	148.8	1015	C / 0.3346	D / 0.2518	-	409
15	**MLR**	STS-2	147.3	1043	A / 0.3045	-	-	368
16	**MLR**	STS-2	148.2	1028	A / 0.5451	B / 0.3762	-	227
	MLR	MP			C / 0.6367	D / 4917	-	
	BRD	S-13	147.6	1040	C / 0.4018	D / 0.5657	-	234
	CVD	S-13	147.8	1036	C / 0.5341	D / 0.4820	-	225
	AMR	S-13	148.3	1032	C / 0.3948	D / 0.3668	-	303
	DRG	MP	148.8	1013	C / 0.6129	D / 0.4398	-	229
	FUL	MP	148.3	1026	C / 0.3074	D / 0.3456	-	359
	GAL	S-13	147.7	1036	C / 0.5839	D / 0.6321	-	188
	GRE	S-13	147.7	1037	C / 0.4429	D / 0.4677	-	250
	LTR	S-13	149.3	1001	C / 0.5873	D / 0.5054	-	226
	MED	MP	148.5	1021	C / 0.2934	D / 0.2466	-	438
	OZU	MP	147.8	1034	C / 0.7640	D / 0.7161	-	155
	SCH	MP	149.1	1006	C / 0.5304	D / 0.2021	-	334
	SIR	S-13	148.0	1031	C / 0.5175	D / 0.5029	-	227
	TES	CMG3T	147.1	1048	C / 0.6320	D / 0.5418	-	189
	VAR	S-13	146.9	1052	C / 0.3719	D / 0.3902	-	287
	VRI	CMG3ESP	147.5	1041	C / 0.8722	D / 0.9228	-	126
17	**MLR**	STS-2	147.9	1040	A / 0.4327	B / 0.2324	-	340
	CFR	S-13	147.0	1056	F / 0.5294	G / 0.4548	-	220
	VRI	S-13	147.3	1052	C / 0.3623	D / 0.2946	E / 0.3015	343
18	**CFR**	S-13	149.0	1024	F / 0.3444	D / 0.3179	-	355
	ISR	S-13	149.8	1003	F / 0.3268	D / 0.2169	-	452
	MLR	S-13	149.9	1002	F / 0.3154	-	-	391
	PPE	S-13	148.4	1036	F / 0.5457	D / 0.6857	-	186
	LTR	S-13	151.0	974	F / 0.3174	D / 0.3809	-	373
19	**CFR**	S-13	147.1	1048	C / 0.1822	D / 0.2137	-	558
	VRI	S-13	147.4	1043	C / 0.6512	D / 0.5793	-	241
	VRI	CMG3ESP			C / 0.3212	D / 0.3080	-	
20	**MLR**	STS-2	148.1	1030	A / 0.2548	-	-	481
	MLR	S-13			C / 0.2800	D / 0.1886	E / 0.1582	
	CFR	S-13	147.1	1048	C / 0.2661	D / 0.2336	E / 0.3744	379
	HARR	S-13	147.5	1040	C / 0.3664	D / 0.3639	E / 0.3895	302
	ISR	S-13	148.0	1031	C / 0.2549	D / 0.1597	E / 0.2221	545
21	**MLR**	STS-2	149.7	996	A / 0.4154	-	-	300

22	**MLR**	S-13	148.4	1030	C / 0.2275	D / 0.2445	E / 0.2348	492
	HARR	S-13	147.9	1040	C / 0.5092	D / 0.6020	E / 0.5358	206
	SNX	S-13	148.7	1024	C / 0.2950	-	-	399
23	**MLR**	STS-2	149.4	1015	A / 0.4281	B / 0.3508	-	225
	MLR	S-13			C / 0.6341	D / 0.6360	E / 0.6162	
	HARR	S-13	148.9	1024	C / 0.5614	D / 0.5793	E / 0.5733	206
	PPE	S-13	147.9	1044	C / 0.4612	D / 0.4846	E / 0.4755	236
	SNX	S-13	149.7	1005	C / 0.6188	D / 0.5156	E / 0.6100	210
	VRI	S-13	148.7	1028	C / 0.6783	D / 0.6740	E / 0.5511	184

Table 3. Values of $\delta t^* = t^*_{df} - t^*_{bc}$ for different frequency bands. **MLR** – GEOFON broad band station at 20 Hz (or 40 Hz) sampling rate (s.r.). *VRI* – Romanian short period telemetered station at ~ 50 Hz s.r. MAN – German-Romanian K2 station at 200 Hz s.r. Frequency bands are the following : A = 0.156 ÷1.875 Hz; B = 0.312 ÷2.031 Hz; C = 0.195÷1.953 Hz; D = 0.391 ÷1.953 Hz; E = 0.391 ÷2.148 Hz; F = 0.195÷1.758 Hz; G = 0.391÷1.758 Hz; H= 0.195÷1.562 Hz

There is also no apparent correlation of Q_P with the type of the recording instrument. The average Q_P value is 295 ± 20 (95% confidence level), with a distribution skewed towards larger values (Fig.5), possibly as a consequence of a hypothesized Q_P increase with depth, discussed below.

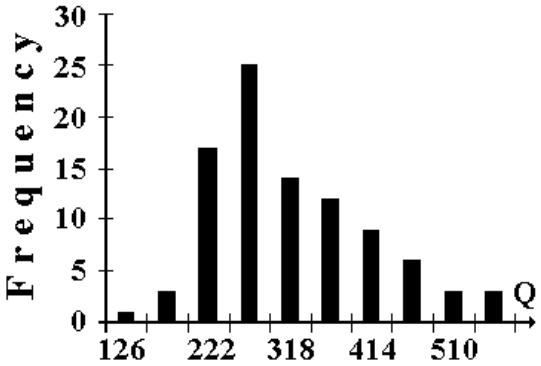

FIG. 5. Histogram of Q_P values.

A plot of Q_P values versus depth of the bouncing point of PKPdf (expressed as the radial distance from the center of the Earth) suggests a possible slight increase of Q_P with depth within the IC (described by the relationship Q_P = 626.8 – 0.325 r_{BP}(km), see also Fig.6) although the large scatter in data prevents a clear result in this respect.

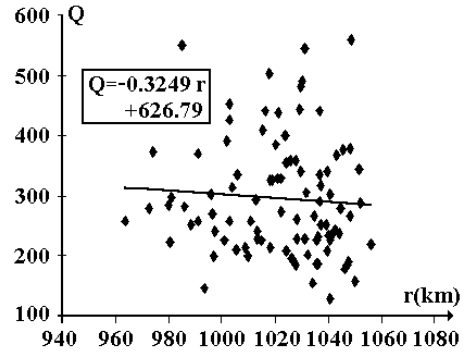

FIG. 6. Q_P values versus radius of the bouncing point of the PKPdf wave.

DISCUSSION

The average value of Q_P is in the range $Q^{-1} \in [0.003, 0.004]$, obtained at 0.2-2 Hz by Cormier (1981) using short-period synthesised seismograms. It is also in a good agreement with the previous results that used spectral ratio method, $Q_P \in [78, 385]$, as reported by Helffrich et al.(2002). However, note that the last result has been obtained by a harmonic mean average of individual Q estimations, while in most of the other studies, including the present one, the arithmetic mean has been used. The observation of a slight increase of Q_P with depth in the IC is in agreement with Tseng et al. (2001) for a ray path centered on the eastern part of the northern Pacific Ocean. It could be regarded as a support for the presence of a mushy zone (a decreasing distribution with depth of liquid inclusions in iron crystals) beneath

IC boundary (Loper and Fearn, 1983; Souriau and Roudil, 1995). Neither the anomalous Q_P value observed by Tseng et al. (2001) using data from the 1996/10/19 Fiji event recorded by the German Regional Seismic Network, nor the exception from linearity of the spectral ratio for paths from south-west Pacific to western Europe (e.g. Souriau and Roudil, 1995) have been observed at the Romanian stations used in this study. However, in a few cases, the best linearity window seems to be reduced to 1-1.5 Hz, leading to a slightly higher value of the slope, up to around $\delta t^* = 1\,\text{second}$.

ACKNOWLEDGEMENTS

The authors express their deep gratitude to Dr. Anca Rosca (MIT), to Dr. Vadim LEVIN (Rutgers University, New Jersey) and to Dr. Vasile Marza (Brasilia University) for very helpful comments and suggestions in their reviews.

REFERENCES

Bonjer, K.-P., Oncescu, M.C., Rizescu, M., Enescu, D., Driad, L., Radulian, M., Ionescu, C., Moldoveanu, T. (2000). Source- and site-parameters of the April 28, 1999 intermediate depth Vrancea earthquake: First results from the new K2 network in Romania, XXVII General Assembly of the European Seismological Commission, Lisbon, Portugal, Book of Abstracts and Papers, SSA-2-13-O, p. 53.

Bhattacharyya, J., Shearer, P. and Master, G., 1993, Inner core attenuation from short period PKP(BC) versus PKP(DF) waveforms, Geophys J. Int., **144**, 1-11.

Buland, R. and Chapman, C.H., 1983, The Computation of Seismic Travel Times, Bull. Seism. Soc. Am., **73**, 1271-1302.

Cormier, V.F., 1981, Short-period PKP phases and the anelastic mechanism

GEOSCOPE PKP data, Geophys J. Int., **123**, 572-587.

Souriau, A., Garcia, R. and Poupinet, G., 2003, The seismological of the inner core, Phys. Earth Planet. Inter., **24**, 291-301.

Doornbos, D.J., 1974, The Anelasticity of the Inner Core, Geophys. J.R. astr. Soc., **38,** 397-415.

Helffrich, G., Kaneshima, S., and Kendall, J.-M., 2002, A local, crossing-path study of attenuation and anisotropy of the inner core, Geophys. Res. Lett., **29**, 1568-1572.

International Seismological Centre, On-line Bulletin, http://www.isc.ac.uk/Bull, Internatl. Seis. Cent., Thatcham, United Kingdom, 2001

Kennett, B.L.N. and Engdahl, E.R., 1991, Travel times for global earthquake location and phase identification, Geophys. J. Int., **105**, 429-465.

Kennett, B.L.N., Engdahl, E.R.and Buland, R., 1995, Constraints on seismic velocities in the Earth from travel times, Geophys J. Int, **122**, 108-124.

Loper, D.E. and Fearn, D.R., 1983, A seismoc model of a partially molten inner core, J. Geophys. Res., **88**, 1235-1242.

Niazi, M. and Johnson, L.R., 1992, Q in the inner core, Phys. Earth Planet Inter., **74**, 55-62.

Roth, E.G., Wiens, D.A., Dorman, L.M., Hildebrand, J. and Webb, S.C., 1999, Seismic attenuation tomography of the Tonga-Fiji region using phase pair methods, J. Geophys. Res., **104**, 4795-4809.

Scherbaum, F. and Johnson, J., 1992, Programmable Interactive Toolbox for Seismological Analysis (PITSA), IASPEI Software Library, Vol. 5.

Souriau, A. and Roudil, P., 1995, Attenuation in the uppermost inner core from broad-band picture of the inner core: structure and rotation, C.R. Geoscience, **335**, 51-63.

Stearn, S.D., 1975, Digital Signal Analysis, Hayden Book Co., Inc., New Jersey.

Tseng, T.L., Huang, B.S. and Chin, B.H. 2001, Depth-dependent attenuation in the uppermost inner core from the Taiwan short period seismic array PKP data, Geophys. Res. Lett., **28**, 459-462.